Available online at www.sciencedirect.com
ScienceDirect
Trans. Nonferrous Met. Soc. China 25(2015) 1097−1105
Transactions of Nonferrous Metals Society of China
www.tnmsc.cn

Microstructure and room temperature tensile property of as-cast Ti44Al6Nb1.0Cr2.0V alloy

Shu-lin DONG, Rui-run CHEN, Jing-jie GUO, Hong-sheng DING, Yan-qing SU, Heng-zhi FU

School of Materials Science and Engineering, Harbin Institute of Technology, Harbin 150001, China

Received 25 May 2014; accepted 1 November 2014

Abstract: The nominal Ti44Al6Nb1.0Cr2.0V alloy was newly designed and prepared by vacuum consumable melting technique with the ingot sizes of *d*225 mm×320 mm. The results show that the average lamella colony size is 780−1830 μm. This as-cast alloy has a modified near lamellar (M-NL) structure that is composed of mainly larger ($\alpha_2+\gamma$) lamella colonies and smaller (B_2+equiaxed γ) blocky morphology. It exhibits the moderate tensile properties at room temperature, in which the Region (5) yields the ultimate tensile strength (UTS) about 499 MPa and the elongation about 0.53%. The obvious brittle fracture characteristics and trans-granular interlamellar fracture are the predominant modes. After room temperature tensile testing, there are some <101] and a few 1/2<112] superdislocations in the γ phase. The as-cast microcrack is the main factor to deteriorate the tensile property, which results in the premature fracture, poor ductility and few dislocations. The addition of Nb, Cr and V can decrease stacking fault energy (SFE) obviously, which is helpful to enhancing the ductility of the alloy.

Key words: titanium aluminum alloy; as-cast; microstructure; tensile property; microcrack

1 Introduction

TiAl-based alloys are considered as the most promising materials for the application in the aviation and aerospace industry due to their low density, high specific strength, excellent high temperature mechanical properties and so on [1−6]. Many kinds of alloying elements, especially the β-stabilizers, such as Nb and Cr, were added to extend the service range of conventional TiAl-based alloys towards higher stress and temperature [7−10]. Many researchers [9,11−14] have proposed high-Nb TiAl-based alloys and lots of researchers focus on it. High-V TiAl-based alloys were proposed by CHEN et al [15,16] recently, in which the typical alloy is Ti43Al9V(Y) (mole fraction, %, similarly hereinafter except the special illustration) with the purpose of improving the deformation processing capacity. The achievements show that Nb can effectively enhance the strength, but decrease the ductility in some degree. On the contrary, Cr, Mn and V can improve the ductility, in which Cr is a more potential element to depress α-transus, substitute Al and enhance ductility in binary TiAl-based alloy compared with other β-stabilizers except Fe [17]. It is also noteworthy that Cr will reduce the ductility of single-phase γ-TiAl alloy [17]. The addition of V is deemed to be helpful for the deformation processing as discussed above; however, it will worsen the oxidation resistance in some degree. While, as well known, B and Y are always used to refine the microstructure of the as-cast TiAl-based alloys including refining the colony size and the interlamellar space, which will be helpful for the mechanical properties according to the Hall−Patch relationship $\sigma_s=\sigma_0+kd^{-1/2}$, where σ_0 and k are the constants related with the crystal types and d is the grain size. Besides the alloying method, there are many other effective methods to improve the microstructure and properties, such as hot isostatic pressing (HIPing), heat treatment (HT), elemental powder metallurgy (EPM) [18], thermo-mechanical treatment (TMT). Thereinto, the TMT method, including forging, extrusion and rolling, is widely used to prepare TiAl-based alloys and it can make the alloys possess excellent mechanical properties, especially at room temperature (RT). Even so, it is necessary to study the as-cast condition firstly, since it can be directly applied

Foundation item: Project (2011CB605504) supported by the National Basic Research Program of China; Project (NCET-12-0153) supported by the Program of New Century Excellent Talents in University; Project (51274076) supported by the National Natural Science Foundation of China
Corresponding author: Rui-run CHEN; Tel/Fax: +86-451-86412394; E-mail: ruirunchen@hit.edu.cn
DOI: 10.1016/S1003-6326(15)63703-7

to producing components and help us to get more knowledge of alloy characterization. Furthermore, the as-cast TiAl-based alloys also possess the advantages of their own. The as-cast processing course usually brings in no or less deformation and there are no substructure induced, thus, it will yield a better creep resistance at the higher service temperature. In this work, the microstructure and tensile properties of the as-cast Ti44Al6Nb1.0Cr2.0V alloy were investigated.

2 Experimental

The alloy with the nominal composition Ti44Al6Nb1.0Cr2.0V was prepared by vacuum consumable melting technique, the ingot was melted two times for the composition homogenization, the diameter and the height of the ingot were about 225 mm and 320 mm, respectively, as shown in Fig. 1. Given the large size of the ingot, the macro-segregation seems to be inevitable. To research the as-cast microstructure and tensile properties, 12 parts were chosen from the ingot in different positions, as shown in Fig. 2.

The compositions were investigated by spectro-fluorimetry method and the oxygen content was tested by oxygen and nitrogen analyzer. Samples for all the testing were prepared firstly by wire-electrode cutting. The phase analysis was conducted by XRD using the Cu K_α radiation (λ=0.154157 nm) and 2θ from 20° to 90°. Scanning electron microscopy (SEM) was used to investigate the alloy characteristics in back-scattered electron (BSE) mode, secondary electron (SE) mode and energy dispersive spectrometer (EDS) mode. The transmission electron microscopy (TEM) was used to investigate microstructure, identify the different phases, determine dislocations Burgers vector after the tensile test and investigate the nanoscale microstructure by high resolution electron microscopy (HREM). The TEM samples were firstly wire-electrode cut into the 300−500 μm foils, then ground to about 100 μm, followed by twin jet electro-polished in a solution of 60% (volume fraction) methanol, 35% butyl alcohol and 5% perchloric acid at 15 V and −30 °C.

The tensile testing at room temperature (RT) was carried out on the 5569-type Instron testing machine with the tensile velocity of 0.5 mm/min. The gauge sizes of the testing samples were 18 mm×5 mm×2 mm.

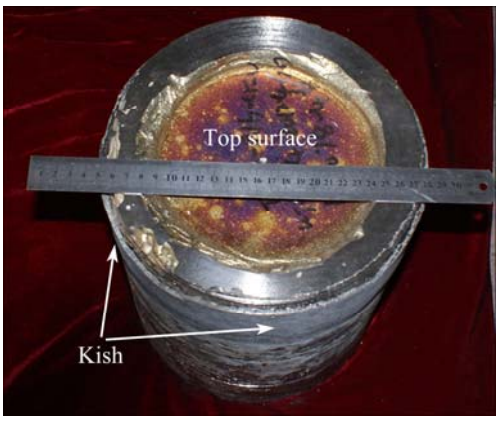

Fig. 1 As-cast ingot prepared by vacuum consumable melting method with sizes of *d*225 mm×320 mm

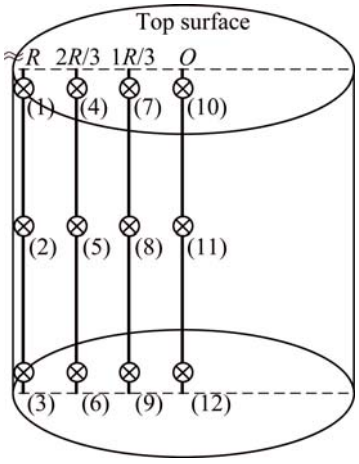

Fig. 2 Schematic diagram of ingot and 12 research positions

3 Results and discussion

3.1 Microstructure of ingot

The actual average chemical composition in positions (1)−(12) is Ti43.98Al5.83Nb1.04Cr2.05V, as well as a small quantity of impurities: Fe<0.05% and Mo<0.02%, which are also the β-stabilizers. The oxygen content is about 680×10^{-6} tested by oxygen and nitrogen analyzer. The average lamella colony sizes (do not consider the segregation in lamella colonies) in different positions are in the range of 780−1830 μm as listed in Table 1 presenting a slight decrease from top to bottom gradually.

Table 1 Average colony size and tensile properties of ingot in 12 different positions

Position No.	Average lamella colony size/μm	Stress/MPa	Strain/%
(1)	1830	400.86	0.53
(2)	1590	440.89	0.49
(3)	1120	410.97	0.31
(4)	1350	468.57	0.50
(5)	1190	498.78	0.53
(6)	780	427.95	0.61
(7)	1650	470.01	0.39
(8)	1540	479.80	0.33
(9)	1030	448.13	0.32
(10)	1680	406.55	0.31
(11)	1420	–	–
(12)	1140	411.18	0.67

Figure 3 shows the XRD pattern of this alloy and the result confirms that it is composed of mainly γ phase, some α_2 and B_2 phases. Figure 4 shows the SEM-BSE images of the as-cast microstructure, in which the (α_2+γ) lamella structure, blocky γ phase and β/α-segregation can be observed [9]. The segregation combining with its surrounding blocky γ phase is the so-called (B_2+ equiaxed γ) blocky morphology [19], in which the α-segregation and its surrounding blocky γ distribute within the colonies, while the β-segregation and the its surrounding blocky γ distribute along the colony boundaries. A modified near lamellar (M-NL) structure is found in this as-cast Ti44Al6Nb1.0Cr2.0V alloy, which is composed of large (α_2+γ) lamella colonies and small (B_2+equiaxed γ) blocky morphology, while the traditional NL structure is composed of large (α_2+γ) lamellar colonies and small blocky equiaxed γ phase. It should be noted that some microcracks are found in the blocky γ as shown in Fig. 4(b). Figure 4 exhibits the SEM-EDS line scanning position and result, which confirms that the white bright contrast B_2 phase contains more β-stabilizers (with the relative high atomic number) and the γ phase contains more Al. Furthermore, it is found that Nb content in different phases does not change as much as that of Cr and V. The result is similar as that studied by KAWABATA et al [1], DING et al [12], KANDRA and LEE [20], and LAPIN et al [21]. This phenomenon is mainly resulted from the fact that Nb is the relatively weak β-stabilizer.

As discussed above, the β-segregation distributes along the colony boundaries or the triple junctions, while

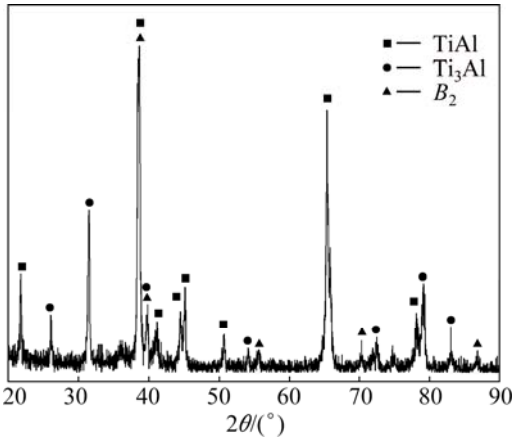

Fig. 3 XRD pattern of as-cast Ti44Al6Nb1.0Cr2.0V alloy

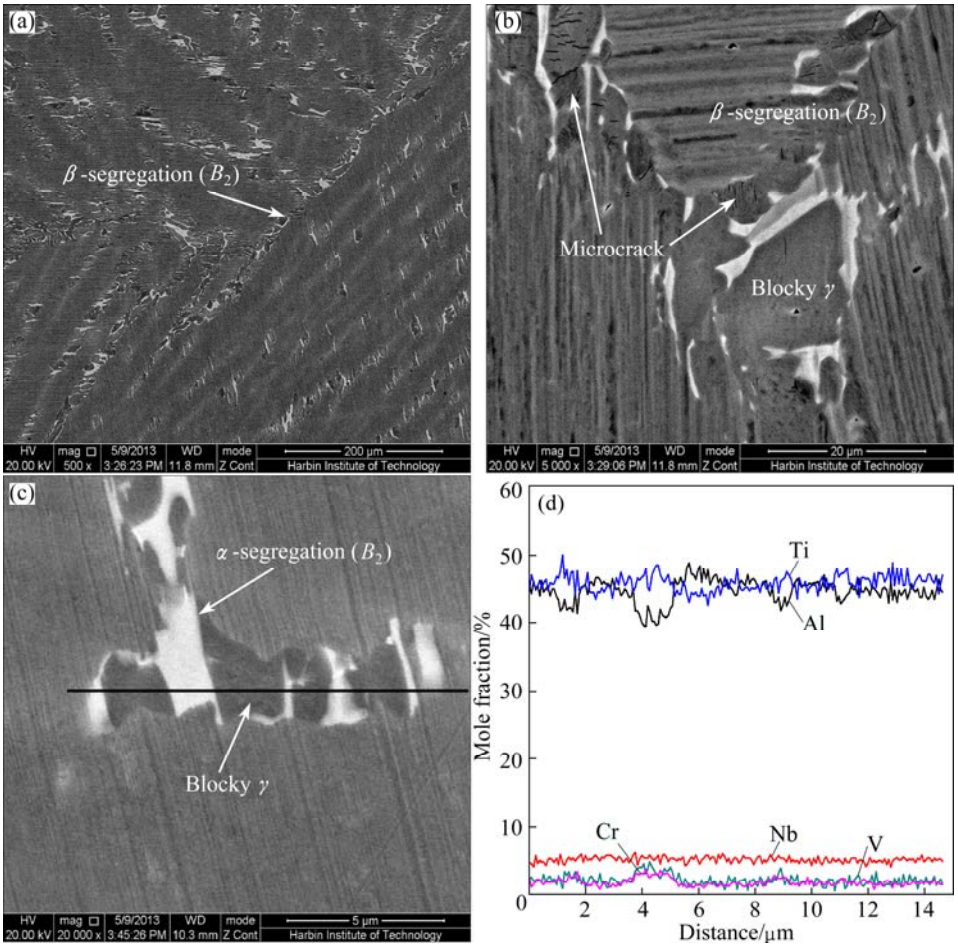

Fig. 4 SEM-BSE images and line scanning by SEM-EDS: (a) Microstructure in lower magnification; (b) Microstructure in higher magnification with some microcrack observed in blocky γ; (c) Microstructure and line scanning path; (d) Line scanning result

the α-segregation distributes within the lamellar colonies [9]. The β-segregation regions may derive from the cores of the primary β grains, while, according to the studies of KIM and DIMIDUK [22] and XU et al [9], α-segregation came from a (α+γ+β) three-phase field below α phase region during cooling for TiAl-based alloys with Nb addition above 9.5%. It was also reported that, for high-V TiAl alloys (such as Ti−45Al−9V alloy), they pass the same solidification route [16]. Although only 6% Nb is added in this alloy, 1.0% Cr and 2.0% V are also contained, all of which are β-stabilizers. Furthermore, there is an empirical equation proposed by SUN et al [23], which is the Cr equivalent formula:

$$[Cr]=Cr+Mn+3/5V+3/8Nb+3/2(W+Mo)+3Fe \quad (1)$$

Equation (1) can be changed into Eq. (2) as follows, which is the Nb equivalent formula:

$$[Nb]=Nb+8/3(Cr+Mn)+8/5V+4(W+Mo)+8Fe \quad (2)$$

Based on Eq. (2), it can be calculated that the equivalent Nb content of Ti44Al6Nb1.0Cr2.0V alloy is about 11.9% (>9.5%). It can be deduced that the same solidification route as above will be passed during cooling [12,16,23−25]. To better understand the solidification route, it can be described in detail as follows [26]:

$$L\rightarrow L+\beta_I\rightarrow\beta_I\rightarrow\beta_I+\alpha\rightarrow$$
$$(\beta_{II}+\gamma_I)+[\text{lamella}(\alpha_2+\gamma_{II})+(\beta_{III}+\gamma_{III})]$$

where β_I is the primary β phase, β_{II} is the residual β_I, β_{III} derives from α phase due to the supersaturation of β-stabilizers. Here, γ_I comes from β_I at high temperature, γ_{II} derives from $\alpha\rightarrow\alpha_2+\gamma$ transformation and γ_{III} may come from β_{III} just like γ_I coming from β_I. It can be concluded that β_{II} is the β-segregation [9] and participates to form the (β_{II}+γ_I) blocky morphology [19] along the colony boundaries or the triple junctions, as shown in Fig. 4(a) and (b). β_{III} is the α-segregation [9] within the lamella colonies and participates to form the (β_{III}+γ_{III}) blocky morphology as shown in Fig. 4(c).

The interlamellar space is affected by many factors, such as the Ti/Al mole ratio, cooling speed, B_2 phase size and its distribution. The average interlamellar space in Region (5) is (1650±1200) nm (the thickness of α_2+γ), which is measured through the TEM observation and the lamella morphology is shown in Fig. 5(a). In the lamella region, the orientation relationships $(0003)_{\alpha_2}//(111)_\gamma$ and $B=[1\bar{2}10]_{\alpha_2}//[01\bar{1}]_\gamma$ were determined, meanwhile, the γ/γ_T structure was found by selected area diffraction

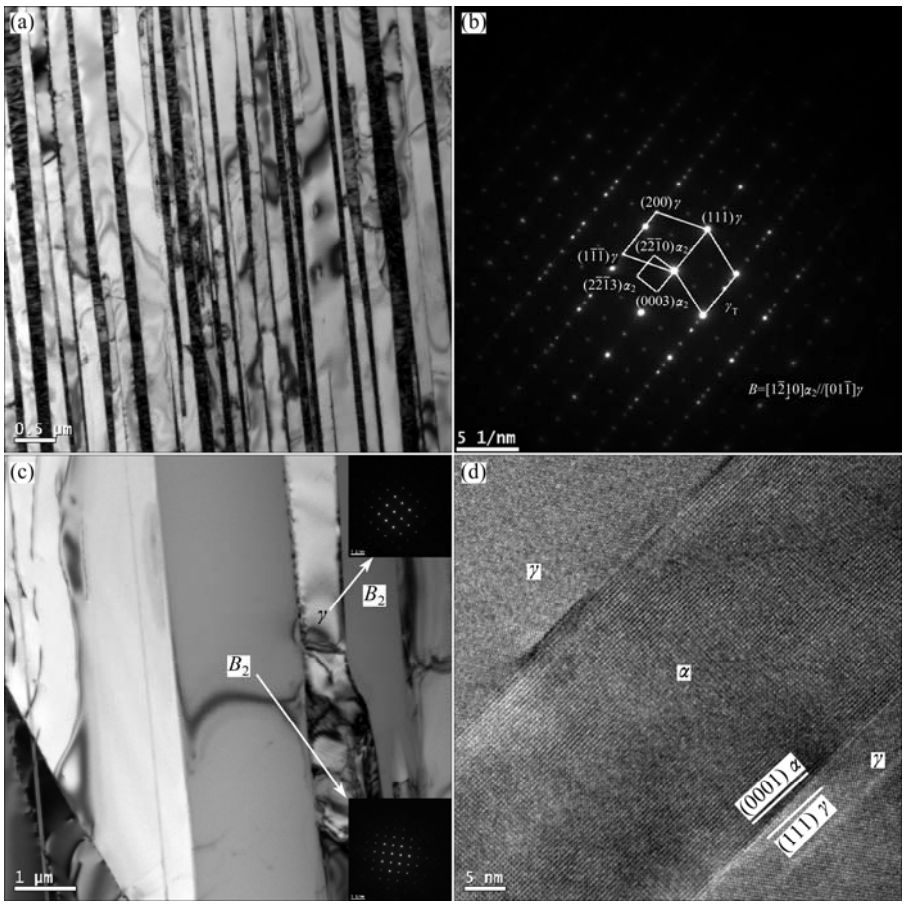

Fig. 5 TEM images in Region (5): (a) (α_2+γ) lamella structure; (b) SADPs of lamella region exhibited in (a) with $B=[1\bar{2}10]_{\alpha_2}//[01\bar{1}]_\gamma$; (c) ($B_2$+$\gamma$) blocky morphology and corresponding SADPs; (d) HREM image in lamella region

patterns (SADPs), as shown in Fig. 5(b). The (B_2+γ) blocky morphology is exhibited in Fig. 5(c), where the B_2 phase, γ phase and their corresponding SADPs are marked. Figure 5(d) shows the HREM image of the lamella region (with the α_2 and γ phase being distinguished by selected area fast Fourier transform (FFT)).

3.2 Tensile properties

As shown in Table 1, the as-cast Ti44Al6Nb1.0Cr-2.0V alloy exhibits the moderate tensile properties at RT. Regions (2), (5) and (8) exhibit the relatively good tensile properties. It can be seen that the inside part of the ingot possesses a better tensile property than that of the outside part. However, in the middle of the ingot, such as Region (11), there are lots of cracks, so that, the unbroken tensile samples cannot be prepared successfully.

The Region (5) yields the ultimate tensile stress (UTS) of 499 MPa or so and the elongation (δ) about 0.53%. Figure 6 exhibits the fracture morphology and profile. Figures 6(a)−(e) show the fracture surface

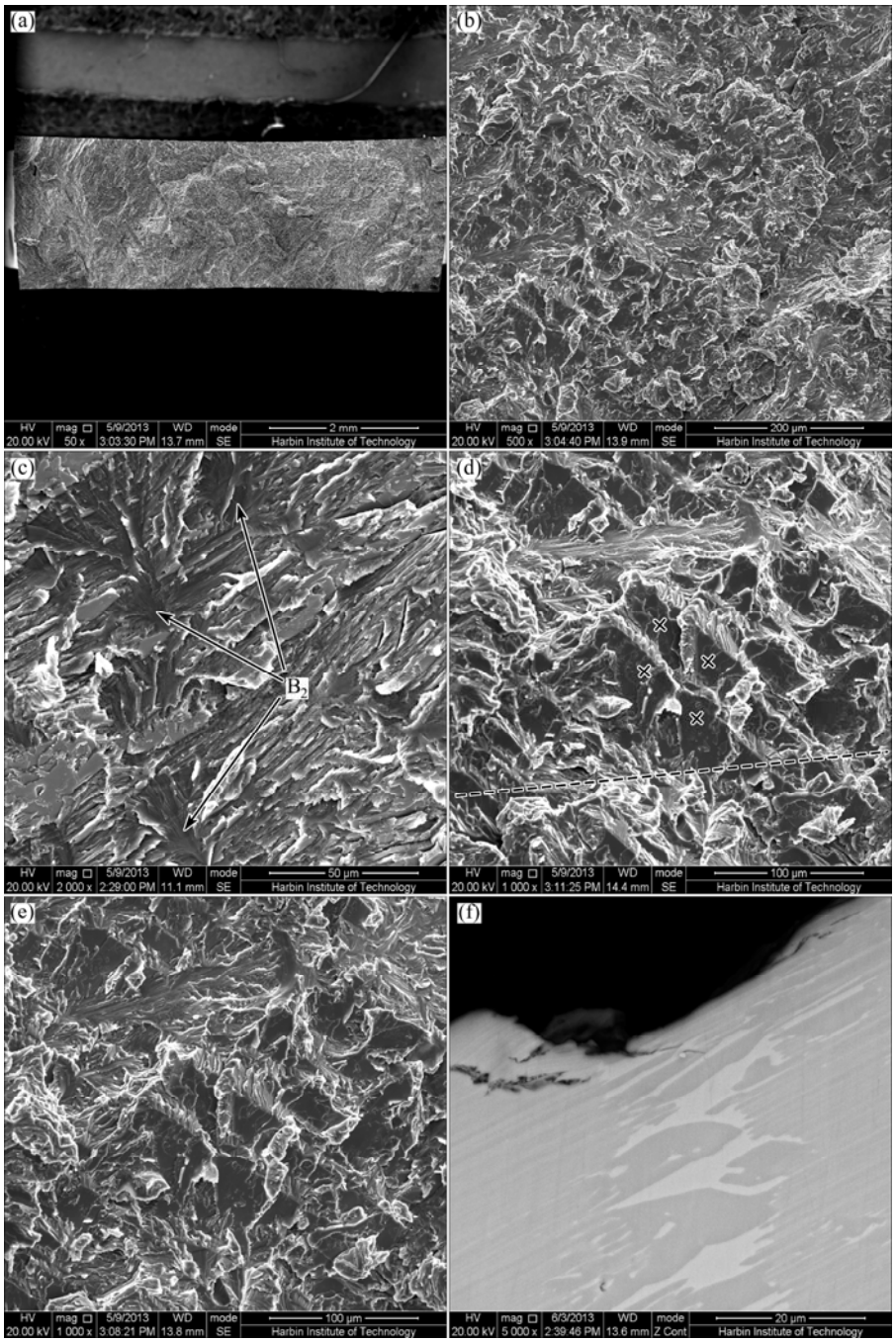

Fig. 6 Fracture morphology and profile: (a) Whole image of fracture surface; (b) Fracture surface under lower magnification; (c) Brittle cleavage fracture of B_2 phase pointed by arrows; (d) Fracture surface under higher magnification with parallel facets marked by cross; (e) Mutually inclined for 30° with dotted line as rotation axis; (f) Fracture profile by SEM-BSE

images observed by SEM-SE, in which, Fig. 6(a) exhibits the whole image of the fracture surface. Figures 6(d) and (e) show the same region, but they are mutually inclining for 30° with the dotted line as the rotation axis. Figure 6(f) shows the SEM-BSE image of the profile.

On the fracture surface, the dimple cannot be found and the groups of parallel facets can help us to understand the low ductility of the as-cast alloy. Trans-granular and interlamellar fracture is widespread, as shown in Figs. 6(b), (d) and (e). Certainly, there are also the trans-granular and tear-lamellar fractures, as shown in Fig. 6(c). Meanwhile, the river shaped pattern (marked by the arrows) can be found and it may form because the B_2 phase was broken and pulled out of the matrix during tensile testing, which implies the brittle cleavage fracture of B_2 phase. In all, the typical brittle fracture mode plays an important role in the testing for this as-cast alloy.

TiAl-based alloys are mainly composed of lamellas, the facets on the fracture surfaces are formed by cleavage along the interlamellar interfaces [27,28], while the contrast of the facets is determined by the angle between the facet normal and incident electron beam. Therefore, if the facets are parallel, they will have the same contrast. In turn, if the facets keep the same contrast in different incident electron beam angles, then these facets are parallel to each other [29]. For instance, for the facets with the same contrast marked with crosses as shown in Fig. 6(d), after tilting by 30°, they still keep the same contrast as shown in Fig. 6(e), which indicates that these facets are parallel mutually. Furthermore, because they are bordered, it implies that these facets may come from the same lamella colony. Figure 6(f) shows the trans-granular and interlamellar fracture mode observed from the sample profile by SEM-BSE.

The microcracks in this as-cast alloy originally exist in blocky γ region, meanwhile, they also easily form in the blocky γ regions, B_2 phase regions or the B_2/γ interface regions during tensile testing due to the dislocation pileup in γ phase, intrinsic brittleness of B_2 phase and stress concentration at B_2/γ interface [30]. So, the ($B_2+\gamma$) blocky morphology regions may evolve to be the crack source. TiAl-based alloy, as a kind of brittle material, is more sensitive to the microcrack. Any kind of microcrack will be catastrophic to its property. The microcracks extending into the colony and spreading along the lamellar structure will deteriorate the tensile property badly. Therefore, how to eliminate or reduce the crack source in an appropriate way is the key work in future. The heat treatment (HT) method seems a good way, but it should be noted that the improper HT technology (for instance, the excessively high temperature or excessively long time) will result in the colony and lamella coarsening, which will also deteriorate the properties. In addition, conventional HT methods are not helpful to eliminating the microcracks, and the hot isostatic pressing (HIPing) seems to be an ideal method [31].

Figure 7 shows the microstructure after RT tensile testing by TEM. Figure 7(a) exhibits the blocky B_2 phase. At RT, the B_2 phase is much harder than the matrix and blocky γ phase and no dislocations are found in it after the tensile testing. Figures 7(b)−(d) show the dislocations and stacking faults (SF) in a relatively thick lamellar γ region (next to B_2 phase) by TEM bright-field (BF) image, in which Fig. 7(b) is observed with B=⟨011⟩, g=⟨200⟩; Fig. 7(c) is with B=⟨011⟩, g=$\langle 11\bar{1}\rangle$ and Fig. 7(d) is with B=⟨001⟩ and g=⟨020⟩.

The SF exists in lamellar γ phase in quantity and they seem to suffer the overlap, since the bright/dark line contrast always changes or disappears. Due to the overlap and long size of the SF, it is hard to estimate the stacking fault energy (SFE), although the SFE is a crucial parameter for material research. However, it can be confirmed qualitatively that this alloy yields a low SFE because of the long SF size according to the formula (3), which is induced by the addition of lots of alloy elements.

$$\gamma=\frac{Gb_1b_2}{8\pi d}\left(\frac{2-\upsilon}{1-\upsilon}\right)\left(1-\frac{2\upsilon\cos 2\alpha}{2-\upsilon}\right) \tag{3}$$

where γ is the SFE, υ is the Poisson ratio, G is the shearing modulus of elasticity, b_1 and b_2 are the Burgers vectors of the two extended dislocations, α is the intersection angle between b and dislocation line, d is the distance between b_1 and b_2.

Via the calculation or consulting the related data, it can be determined that there are <101] and 1/2<112] superdislocations in the BCC γ phase. For instance, as shown in Fig. 7(b), the dislocations marked 1 have the Burger's vector $<10\bar{1}]$, since it is visible with g=⟨200⟩, g=$\langle 11\bar{1}\rangle$ and invisible with g=⟨020⟩. The dislocation marked 2 is visible with g=⟨200⟩, g=⟨020⟩ and invisible with g=$\langle 11\bar{1}\rangle$, so it seems to be the $<1\bar{1}0]$ ordinary dislocations. But it is visible with g=⟨220⟩ (not shown here), so it is determined to be the 1/2<112] superdislocation finally. At RT, the Peierls stress that can hinder the dislocations slipping is usually higher for the TiAl-based alloys. However, the <101] superdislocation suffers relatively low Peierls stress. So, the <101] superdislocation is more easily to move. In addition, a few 1/2<112] superdislocations are also found. The result is as the same as that found by WU and HWANG [32], LIU et al [33], and SUN et al [23]. The fewer slip systems and dislocations imply the lower ductility; however, as discussed above, the alloy has low SFE and it should be usually corresponding to a high ductility,

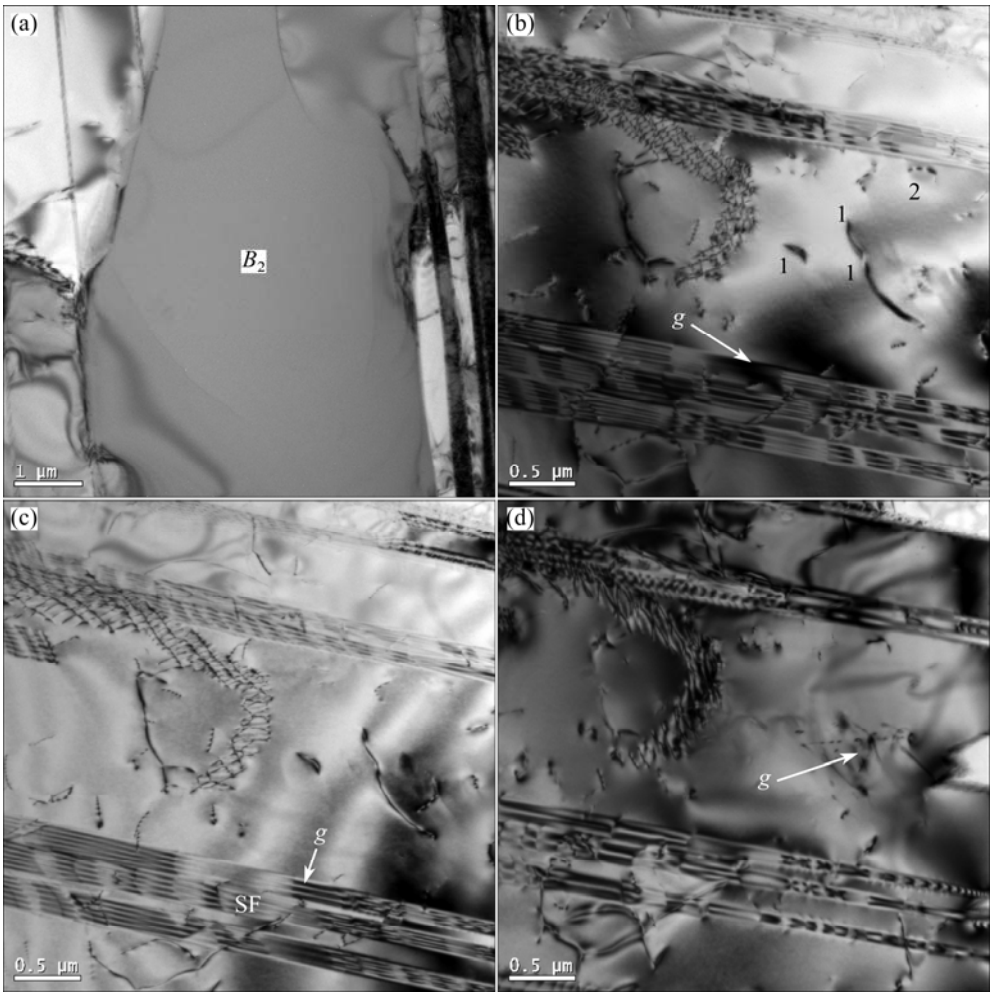

Fig. 7 TEM images exhibiting B_2 phase region after RT tensile testing (a) and dislocations in γ phase by bright-field image (b−d): (b) With B=⟨011⟩ and g=⟨200⟩; (c) With B=⟨011⟩ and g=$\langle 1\,1\,\bar{1}\rangle$; (d) With B=⟨001⟩ and g=⟨020⟩

because the low SFE can facilitate dislocations to extend and slip, and be conducive to the formation of twin crystals and so on. This contradiction implies that there must be some other reasons to lead the premature fracture and moderate tensile property of this as-cast alloy, in which the crack source as discussed above may be the most imperative factor. After the proper post processing aim at eliminating the crack source, the alloy properties will be improved, meanwhile, the measurement and calculation of critical resolved shear stress (CRSS) and SFE are also necessary, since they are the significant parameters for material research [34,35].

4 Conclusions

1) The as-cast Ti44Al6Nb1.0Cr2.0V alloy ingot is prepared by vacuum consumable melting technique with the average colony size of 780−1830 μm. It has a modified near lamellar (M-NL) structure composed of (α_2+γ) lamellar colonies and (B_2+equiaxed γ) blocky morphology along the colonies boundaries or within the colonies. The γ/γ_T structure is also found in the lamella region and the average interlamellar space in Region (5) is (1650±1200) nm.

2) The as-cast alloy has a moderate tensile property at RT with the UTS about 499 MPa and the elongation about 0.53% for the sample in Region (5). It exhibits the obvious brittle fracture characteristics. Trans-granular interlamellar fracture is the predominant mode.

3) The blocky (B_2+γ) region can evolve to be the crack source, which is due to the microcrack in blocky γ, the intrinsic brittleness of B_2 phase, dislocation pileup in blocky γ phase and stress concentration at B_2/γ interface originally exists.

4) Some 1/2<112] and <101] superdislocations are found. The addition of Nb, Cr and V can decrease SFE obviously, which indicates that the as-cast alloy should have a potential on ductility enhancement.

References

[1] KAWABATA T, TAMURA T, IZUMI O. Effect of Ti/Al ratio and Cr,

Nb, and Hf additions on material factors and mechanical properties in TiAl [J]. Metallurgical and Materials Transactions A, 1993, 24: 141−150.

[2] HUANG Lan, LIAW P K, LIU CT, LIU Yong, Huang Jin-song. Microstructural evolution of (TiAl)+Nb+W+B alloy [J]. Transactions of Nonferrous Metals Society of China, 2011, 21(10): 2192−2198.

[3] DING Xian-fei, LIN Jun-pin, ZHANG Lai-qi, CHEN Guo-liang. Effect of heat treatment on microstructure of directionally solidified Ti−45Al−8Nb−(W,B,Y) alloy [J]. Transactions of Nonferrous Metals Society of China, 2011, 21(1): 26−31.

[4] WANG Yan, LIU Yong, YANG Guang-yu, LI Hui-zhong, TANG Bei. Microstructure of cast γ-TiAl based alloy solidified from β phase region [J]. Transactions of Nonferrous Metals Society of China, 2011, 21(2): 215−222.

[5] DING X F, LIN J P, ZHANG L Q, SONG X P, CHEN G L. Microstructure and mechanical properties of directionally solidified Ti−45Al−8Nb−(W,B,Y) alloys [J]. Materials & Design, 2011, 32: 395−399.

[6] ZHOU Y, SUN D L, JIANG D P, HAN X L, WANG Q, WU G H. Microstructural characteristics evolution of Ti_2AlN/TiAl composites with a network reinforcement architecture during reaction hot pressing process [J]. Materials Characterization, 2013, 80: 28−35.

[7] YANG Xin, XI Zheng-ping, LIU Yong, TANG Hui-pin, HU Ke, JIA Wen-peng. Microstructure and fracture toughness of a TiAl−Nb composite consolidated by spark palsma sintering [J]. Transactions of Nonferrous Metals Society of China, 2012, 22(11): 2628−2632.

[8] JUNG I S, JANG H S, OH M H, LEE J H, WEE D M, Microstructure control of TiAl alloys containing β stabilizers by directional solidification [J]. Materials Science and Engineering A, 2002, 329−331: 13−18.

[9] XU X J, LIN J P, TENG Z K, WANG Y L, CHEN G L. On the microsegregation of Ti−45Al−(8−9)Nb−(W,B,Y) alloy [J]. Materials Letters, 2007, 61: 369−373.

[10] LAPIN J, GABALCOVA Z. Solidification behaviour of TiAl-based alloys studied by directional solidification technique [J]. Intermetallics, 2011, 19: 797−804.

[11] CHENG T T, WILLIS M R. Effects of aging on the microstructure and creep properties of γ-TiAl containing heavy alloying [J]. Scripta Materialia, 1998, 39: 1255−1265.

[12] DING X F, LIN J P, ZHANG L Q, WANG H L, HAO G J, CHEN G L. Microstructure development during directional solidification of Ti−45Al−8Nb alloy [J]. Journal of Alloys and Compounds, 2010, 506: 115−119.

[13] DING X F, LIN J P, ZHANG L Q, SU Y Q, WANG H L, CHEN G L. Lamellar orientation control in a Ti−46Al−5Nb alloy by directional solidification [J]. Scripta Materialia, 2011, 65: 61−64.

[14] DING X F, LIN J P, ZHANG L Q, SU Y Q, CHEN G L. Microstructural control of TiAl−Nb alloys by directional solidification [J]. Acta Materialia, 2012, 60: 498−506.

[15] CHEN Y Y, LI B H, KONG F T. Microstructural refinement and mechanical properties of Y-bearing TiAl alloys [J]. Journal of Alloys and Compounds, 2008, 457: 265−269.

[16] LI B H, CHEN Y Y, HOU Z Q, KONG F T. Microstructure and mechanical properties of as-cast Ti−43Al−9V−0.3Y alloy [J]. Journal of Alloys and Compounds, 2009, 473: 123−126.

[17] HUANG S C, HALL E L. The effects of Cr additions to binary TiAl-base alloys [J]. Metallurgical and Materials Transactions A, 1991, 22: 2619−2627.

[18] LI Xue-wen, SUN Hong-fei, FANG Wen-bin, DING Yong-feng. Structure and morphology of Ti−Al composite powders treated by mechanical alloying [J]. Transactions of Nonferrous Metals Society of China, 2011, 21(S2): s338−s341.

[19] XU X J, LIN J P, WANG Y L, GAO J F, LIN Z, CHEN G L. Microstructure and tensile properties of as-cast Ti−45Al−(8−9)Nb−(W,B,Y) alloy [J]. Journal of Alloys Compounds, 2006, 414: 131−136.

[20] KANDRA J T, LEE E W. Temperature and microstructural dependence of the deformation of a high Nb Ti−Al alloy [J]. Metallurgical and Materials Transactions A, 1994, 25: 1667−1679.

[21] LAPIN J, GABALCOVA Z, PELACHOVA T. Effect of Y_2O_3 crucible on contamination of directionally solidified intermetallic Ti−46Al−8Nb alloy [J]. Intermetallics, 2011, 19: 396−403.

[22] KIM Y W, DIMIDUK M D. Progress in the understanding of gamma titanium aluminides [J]. Journal of The Minerals Metals & Materials Society, 1991, 43: 40−47.

[23] SUN F S, CAO C X, KIM S E, LEE Y T, YAN M G. Alloying mechanism of beta stabilizers in a TiAl alloy [J]. Metallurgical and Materials Transactions A, 2001, 32: 1573−1589.

[24] JOHNSON D R, INUI H, YAMAGUCHI M. Crystal growth of TiAl alloys [J]. Intermetallics, 1998, 6: 647−652.

[25] SUN H L, HUANG Z W, ZHU D G, JIANG X S. Dendrite core grain refining and interdendritic coarsening behaviour in W-containing γ-TiAl based alloys [J]. Journal of Alloys and Compounds, 2013, 552: 213−218.

[26] DONG S L, CHEN R R, GUO J J, DING H S, SU Y Q, FU H Z. Microstructure control and mechanical properties of Ti44Al6Nb1.0Cr2.0V alloy by cold crucible directional solidification [J]. Materials Science and Engineering A, 2014, 614: 67−74.

[27] CHAN K S, ONSTOTT J, KUMAR K S. The Fracture resistance of a binary TiAl alloy [J]. Metallurgical and Materials Transactions A, 2000, 31: 71−80.

[28] HU D, HUANG A, JIANG H, MOTA S N, WU X H. Pre-yielding and pre-yield cracking in TiAl-based alloys [J]. Intermetallics, 2006, 14: 82−90.

[29] HU D, JIANG H, WU X. Microstructure and tensile properties of cast Ti−44Al−4Nb−4Hf−0.1Si−0.1B alloy with refined lamellar microstructures [J]. Intermetallics, 2009, 17: 744−748.

[30] CHEN J H, WANG G Z, ZHANG J. Study on notch fracture of TiAl alloys at room temperature [J]. Metallurgical and Materials Transactions A, 2004, 35: 439−457.

[31] LIU G, ZHANG G J, JIANG F, DING X D, SUN Y J, SUN J, MA E. Nanostructured high-strength molybdenum alloys with unprecedented tensile ductility [J]. Nature Materials, 2013, 12: 344−350.

[32] WU Y, HWANG S K. Microstructure refinement and improvement of mechanical properties and oxidation resistance in EPM TiAl-based intermetallics with yttrium addition [J]. Acta Materialia, 2002, 50: 1479−1493.

[33] LIU Z C, LIN J P, LI S J, CHEN G L. Effects of Nb and Al on the microstructures and mechanical properties of high Nb containing TiAl base alloys [J]. Intermetallics, 2002, 10: 653−659.

[34] ZHANG W J, APPEL F. Effect of Al content and Nb addition on the strength and fault energy of TiAl alloys [J]. Materials Science and Engineering A, 2002, 329−331: 649−652.

[35] ZHANF W J, LIU Z C, CHEN G L, KIM Y W. Deformation mechanisms in a high-Nb containing γ-TiAl alloy at 900 °C [J]. Materials Science and Engineering A, 1999, 271: 416−423.

铸态 Ti44Al6Nb1.0Cr2.0V 合金的显微组织及室温拉伸性能

董书琳，陈瑞润，郭景杰，丁宏升，苏彦庆，傅恒志

哈尔滨工业大学 材料科学与工程学院，哈尔滨 150001

摘　要：设计了新型 Ti44Al6Nb1.0Cr2.0V 合金，并采用真空自耗法熔炼制备尺寸为 *d*225 mm×320 mm 的合金锭。结果表明，其层片厚度在 780~1830 μm 范围。此合金表现为一种改进的近片层(M-NL)微观结构，主要由(α_2+γ)层片结构和较多的(B_2+等轴 γ)小块状结构组成。合金的室温拉伸性能适中，在选取的 12 个研究位置中，5#位置其平均性能达到 UTS=499 MPa 和 σ=0.53%。合金表现出明显的脆性断裂特征，其中穿晶穿片层断裂模式较为普遍。室温拉伸实验后，在 γ 相中可以观察到<101] 和 1/2<112] 超位错。大量 Nb、Cr、V 等元素的加入造成了合金较低的堆垛层错能，这对合金塑性的提升是有益的，但铸造微裂纹导致了合金提早断裂，对性能造成很大影响。

关键词：钛铝合金；铸态；微观结构；拉伸性能；微裂纹

(Edited by Xiang-qun LI)